Transferrin Decorated Thermoresponsive Nanogels as Magnetic Trap Devices for Circulating Tumor Cells

Mazdak Asadian-Birjand, Catalina Biglione, Julian Bergueiro, Ariel Cappelletti, Chinmay Rahane, Govind Chate, Jayant Khandare, Bastian Klemke, Miriam C. Strumia, Marcelo Calderón*

A rational design of magnetic capturing nanodevices, based on a specific interaction with circulating tumor cells (CTCs), can advance the capturing efficiency and initiate the development of modern smart nanoformulations for rapid isolation and detection of these CTCs from the bloodstream. Therefore, the development and evaluation of magnetic nanogels (MNGs) based on magnetic nanoparticles and linear thermoresponsive polyglycerol for the capturing of CTCs with overexpressed transferrin (Tf^+) receptors has been presented in this study. The MNGs are synthesized using a strain-promoted "click" approach which has allowed the in situ surface decoration with Tf–polyethylene glycol (PEG) ligands of three different PEG chain lengths as targeting ligands. An optimal value of around 30% of cells captures is achieved with a linker of eight ethylene glycol units. This study shows the potential of MNGs for the capture of CTCs and the necessity of precise control over the linkage of the targeting moiety to the capturing device.

M. Asadian-Birjand, Dr. J. Bergueiro, Prof. M. Calderón
Institute of Chemistry and Biochemistry
Freie Universität Berlin
Takustr. 3, 14195 Berlin, Germany
E-mail: marcelo.calderon@fu-berlin.de
C. Biglione, Dr. A. Cappelletti, Prof. M. C. Strumia
LAMAP Laboratorio de Materiales Poliméricos
IMBIV-CONICET
Departamento de Química
Facultad de Ciencias Químicas
Universidad Nacional de Córdoba
Haya de la Torre y Medina Allende
X5000HUA, Córdoba, Argentina
C. Rahane, G. Chate, Prof. J. Khandare
MAEER's Maharashtra Institute of Pharmacy
Kothrud, Pune 411038, Maharashtra, India
Dr. B. Klemke
Helmholtz-Zentrum Berlin für Materialien und Energie GmbH
D-14109 Berlin, Germany

1. Introduction

The advanced stage of cancer is known as metastasis. At this point subgroups of cancer cells leave the primary tumor, migrate through blood circulation, and colonize new distant tissue forming a new tumor mass.[1] These metastases, not the primary tumors, cause about the 90% of cancer deaths. Therefore, the early identification of cancer cells that are traveling through the blood circulation, so-called circulating tumor cells (CTCs), is crucial to the success of cancer therapy and to the improvement of patients' survival rates.[2] Since CTCs are extremely rare in the bloodstream, their detection from the background of hematologic cells is quite challenging.[3] Currently, there are several approaches both on the market and under trial that improve the isolation and enrichment as well as the detection of CTCs out of blood samples and in

DOI: 10.1002/marc.201500590

vivo.[3,4] Between them, most isolation and detection techniques used are based on Velcro-like devices,[5] microfluidic devices, such as CTC-chips,[6] DEPArray system,[7] and chaotic micromixers,[8] or CTC enrichment methods such as electrokinetic enrichment devices,[9] and CellCollector.[10] Also immunochemistry-based nanoparticles are used in systems such as CellSearch,[11] and MagSweeper can identify and trap CTCs from whole blood.[12] These systems are based on antibody coated magnetic nanoparticles (MNPs) that stick to the epithelial cell adhesion molecule (EpCAM) protein that is expressed on the tumor cells. Considering the limitations of antibody-based CTC capturing assays, such as not capturing CTCs that lack the EpCAM protein or CTCs that have gone through the epithelial-to-mesenchymal transition,[13] an improvement in the efficiency in CTC capturing efficiency relies on the smart design and fabrication of CTC catching nanodevices.[14] Their design with respect to the elasticity, stability, size, and shape has a strong impact on their interaction with biomaterials such as circulating cells.[15–19] A class of systems that allows a reproducible synthetic control over these parameters are so-called nanogels (NGs).[20,21] These systems are defined as nanometric aqueous dispersions of hydrogel particles, which are formed by physically or chemically crosslinked polymer network chains. NGs have shown many interesting intrinsic properties, such as elastic nature, high water content, flexibility, excellent water dispersibility/solubility, and cell and tissue compatibility. Combination of MNPs with NGs has enabled many opportunities for their utilization in the biomedical field including cellular imaging, hyperthermia, and advanced drug delivery.[22] Nevertheless, the design of the NGs in terms of how the nanoparticles are incorporated into the NG is of high importance for their function as a magnetic trap of CTCs. The use of MNPs as the network crosslinker could ensure a high amount of MNPs embedded into the NG matrix that reveal an optimal magnetic strength.

As an alternative to widely used antibodies, the glycoprotein transferrin (Tf) can be used as the model targeting ligand as it is well known that the Tf receptor concentration on many tumor phenotype cells is much higher than that on normal cells.[23,24] In a previous study we designed a Tf conjugated magneto-dendritic nanosystem for rapid and efficient capture of Tf receptor-overexpressing (TfR+) cancer cells from an artificial CTC-like suspension. We were able to isolate captured cells from peripheral blood cells and perform high-resolution imaging.[25] In the present study, we hypothesize that NG platform could enhance cell interactions and result in an effective CTC capture because of the NG's outstanding cell and tissue compatibility due to their soft nature.[26,27] Moreover, we were interested in investigating their interaction to CTCs by changing the distances between targeting ligands and nanogel. Therefore, a synthetic methodology was developed that generated magnetic nanogels (MNG) with low polydispersibility and reproducibility, and that allowed their decoration with targeting ligands in situ to evaluate them for capturing CTCs.

2. Results and Discussion

The synthesis of NGs is typically based on templates which afford the generation of a crosslinked network in a confined nanotemplated space. The crosslinked network could be generated by nanoprecipitation through orthogonal strain-promoted azide-alkyne cycloaddition (SPAAC), which enabled the selective ligation with minimum purification steps, in situ incorporation of bioactives, and without the presence of stabilizer. We therefore decided to use a modification of this technique for the synthesis of MNGs as shown in Figure 1. We first synthesized the building blocks, namely, thermoresponsive linear polyglycerol (tPG), magnetic nanoparticles decorated with bicyclononyne (MNPs@BCN), and Tf functionalized polyethylene glycols (PEGs) linker (Tf-PEG$_x$-N$_3$).

2.1. tPG Synthesis

tPG was chosen as the polymer network chain due to its known biocompatible profile,[28,29] its tunable character,[30] and its outstanding qualities as a building block for nanogel formation as shown in a previous work from our group. Therefore, according to the reported methodogy, tPG-azide with an average molecular weight of 5 kDa was utilized in MNG synthesis (Figure 1a i).[31]

2.2. MNPs@BCN Synthesis

Bare MNPs were synthesized based on a modification of an already reported methodology (Figure 1a ii),[32] to obtain low polydisperse spherical particles with an average diameter of 10 ± 3 nm as observed in transmission electron microscopy (TEM) images (Table S1, Supporting Information). Zeta potential gave positive values as expected. MNPs were functionalized with aminopropyl triethoxysilane (APTES) with an improved methodology based on ultrasonication.[33] We used an ultrasonication horn to increase the energy on the coating process and prevent even more aggregation of the MNPs (Figure 1a ii). There were no significant changes in the zeta potential values due to the terminal amines of the APTES. Also the size of the particles by transmission electron microscopy did not show any relevant change. APTES incorporation was confirmed by Fourier transform infrared spectroscopy (FT-IR) with the appearance of the silane characteristic signals at 1200 cm^{-1} (Table S1, Supporting Information). The number of amines per nanoparticle was

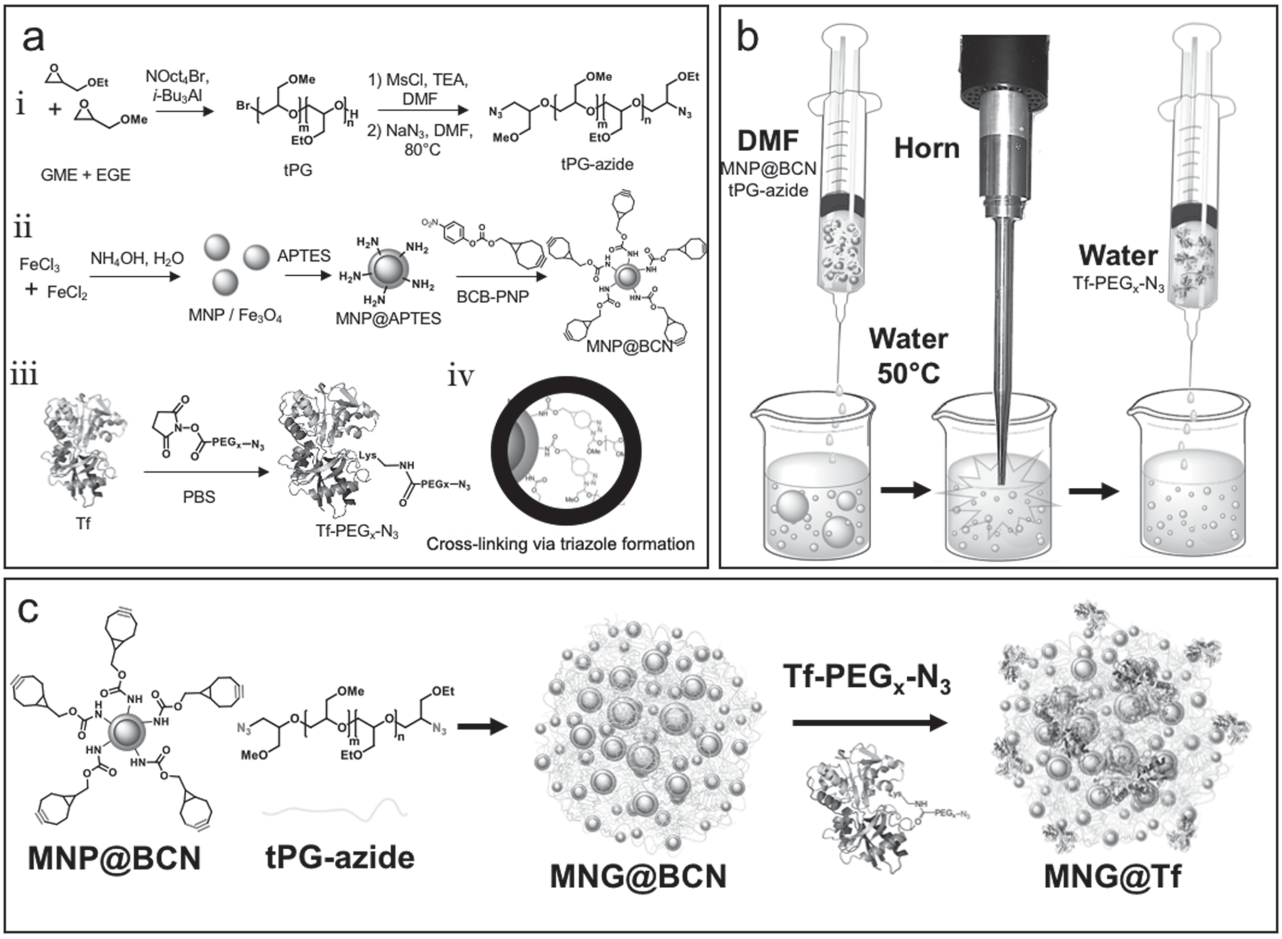

Figure 1. MNG construction scheme. a) Synthesis of macromonomers such as (i) tPG-azide through polymerization of glycidyl methyl ether (GME) and ethyl glycidyl ether (EGE), (ii) **MNP@BCN**, and (iii) **Tf-PEG$_x$-N$_3$**. (iv) Demonstration of crosslinking chemistry for nanogel formation. b) MNG synthesis procedure through ultra sound assisted thermo-nanoprecipitation and c) the reaction agents involved.

calculated by colorimetric titration of APTES amines with picric acid and nanoparticle calculation by nanotracking analysis (NTA) giving a value of around five amine groups per nanoparticle (Supporting Information). The **MNPs@APTES** were decorated with bicyclononyne (BCN) moieties through a nucleophilic attack of the APTES terminal amine to BCN-paranitrophenyl carbonate (BCN-PNP) resulting in carbamate formation between **MNP@APTES** and BCN (Figure 1aii). BCN modification was confirmed by the appearance of the alkynyl signal at 2100 cm^{-1} and a C–H signal at 2900 cm^{-1} in FT-IR as well as for the change to negative values of zeta potential after reaction (Table S1, Supporting Information). Moreover, the BCN groups were quantified by an UV-vis spectrophotometry test through **MNP@BCN** conjugation to an azido dansyl dye after magnetic workup. Almost the same amount of BCN moieties as amines in **MNP@APTES** were calculated, confirming a quantitative functionalization of the amine reactive groups on APTES surface (Table S1, Supporting Information). This led to the conclusion that **MNP@BCN** was a suitable crosslinker and anchoring point for strain-promoted cycloaddition.

2.3. Tf-PEG$_x$-N$_3$ Linker Synthesis

For the decoration with Tf targeting ligands, we were interested in investigating the influence of the different linker distances between the MNG and the targeting ligand on the cell capturing efficiency. To obtain these different distances, a heterobifunctional azido-PEG-N-hydroxysuccinidime (**N$_3$-PEG$_x$-NHS**) linker with three different ethylene glycol repeating units (x = 4, 8, and 12) was chosen. The conjugation was achieved by amide bond formation between lysine moieties of the Tf protein and *N*-hydroxysuccinimidyl (NHS) of the linker, which obtained a free azido group on the Tf for further conjugation to the MNG (Figure 1aiii). The **Tf-PEG$_x$-N$_3$** conjugates were purified from the non-reactive free linker by dialysis against water with a membrane of a molecular weight cut-off of 50 kDa. Due to the huge difference in molecular weights of the

linkers to the Tf, it was not trivial to determine the conjugation efficiency of the linker to the protein directly. Since Tf possesses approximately 60 lysine moieties in its structure, we explored five different feed ratios of linker to Tf (1:1, 2:1, 5:1, 10:1, 20:1) and compared them to the experimental values obtained by MALDI-TOF mass spectrometry and ^{1}H-NMR spectroscopy to be able to precisely determine the conjugation efficiency (Figures S3–S6, Supporting Information). The slopes that were obtained from linear regression revealed the conjugation efficiency of each of the linker-conjugates. The values obtained for the smaller linkers **N_3-PEG_4-NHS** and **N_3-PEG_8-NHS** were low, 13.34% and 12.05%, respectively, while the highest value of 44.92% was surprisingly achieved for **N_3-PEG_{12}-NHS** (Figure S6, Supporting Information). FT-IR spectroscopy showed the appearance of the azide signal at 2099 cm^{-1} for the conjugates after workup. For all conjugates no changes were observed for the tertiary structure of Tf as observed in circular dichroism (CD) in the range between 190 and 240 nm which indicated that the conjugation chemistry had no influence on Tf's structural integrity (Figure S7, Supporting Information).

2.4. Synthesis and Characterization of MNGs@Tf

The MNG's building blocks were **MNPs@BCN** that served both as the nanogel crosslinker and anchoring point for the targeting moiety, tPG-azide as thermoresponsive polymer network, and **Tf-PEG_x-N_3** as targeting moieties with different lengths (Figure 1). For the synthesis of MNGs, we developed a horn ultrasonication assisted methodology based on thermo nanoprecipitation[31] that yielded defined and dispersed MNGs in a fast, clean, and surfactant free manner (Figure 1b). Horn sonication assistance allowed us to gain control over the aggregation behavior that was obtained if nanoparticles reactions were preformed with a magnetic stirrer or even in an ultrasonication bath. Copper-free orthogonal strain-promoted azide-alkyne cycloaddition was selected as the gelification reaction. In the MNG formation, **MNP@BNC** and tPG-azide were crosslinked and the remaining BCN moieties were quenched with the three synthesized **Tf-PEG_x-N_3** conjugates (Figure 1c). This way we synthesized **MNG1**, which was only quenched with azido propanol and served as a non-targeting control (Table 1). Moreover, three nanogels were produced and quenched with the three linkers of different lengths, namely, **Tf-PEG_4–N_3** (**MNG2**), **Tf-PEG_8-N_3** (**MNG3**), and **Tf-PEG_{12}-N_3** (**MNG4**), all with a PEG-to-Tf ratio of 1:1. Both the crosslinking and the quenching reactions were checked via FT-IR spectroscopy. The disappearance of the azide signal at 2099 cm^{-1} indicated the successful strain promoted cycloaddition completion. The Tf decorated MNGs (**MNG@Tf**) were all dispersible in water and obtained mean hydrodynamic diameters in the range of 100–200 nm as reflected when analyzed with NTA (Table 1). As an example, **MNG4** showed a hydrodynamic diameter of 116 ± 57 nm in NTA (Figure 2c). Similar diameters to those observed by NTA, were recorded when **MNG4** was visualized by TEM and scanning electron microscopy (SEM) (Figure 2a,b). Thermoresponsiveness of the nanogels was determined by a temperature-trend dynamic light scattering (DLS) experiment and revealed a volume phase transition temperature (VPTT) of 42 °C. **MNG1** magnetic properties were analyzed in terms of magnetization versus field and temperature, as well as through magnetic resonance imaging measurements. The zero hysteresis of the magnetization curve at a zero magnetic field indicated the superparamagnetic properties of **MNG1** (Figure 2d). As expected, when compared to the seed bare **MNPs** (64 emu g^{-1}), the **MNG4** (44 emu g^{-1}) showed a lower magnetization values at 20 000 Oe, because **MNG4** also consists of nonmagnetic polymer parts that contributed to its applied weight (Figure 2d). Moreover, as we used a thermoresponsive polymer in the construction of the MNGs, we also analyzed the effect of temperature to the magnetic behavior (Figure 2e). The magnetization linearly increased with the temperature and was not affected near the VPTT of the tPG. In light of the magnetic properties, the MNGs potential use as a magnetic resonance imaging (MRI) contrast agent was demonstrated by collecting MRI images on a 7 T Bruker BioSpec 70/20 USR. As shown in

Table 1. **MNG@Tf** characteristics.

Sample	Size[a] [nm]	Tf-PEG_x-N_3 PEG chain length [ethylene glycol units]	Tf-PEG_x-N_3 PEG-to-Tf weight ratio[b]	Tf-PEG_x-N_3 conjugation efficiency to MNG [%]	Tf amount per MNG[c] [nmol mg^{-1}]	MNG reaction yields [wt%]	MNG cell capturing efficiency [%]
MNG1	233 ± 93	–	–	–	–	20	13
MNG2	165 ± 87	4	1:1	90	120	33	23
MNG3	112 ± 99	8	1:1	90	7.6	92	33
MNG4	116 ± 57	12	1:1	64	9.3	52	7

[a]Hydrodynamic diameter obtained through NTA; [b]Ratio based on detected mass by MALDI-TOF; [c]Concentration obtained spectroscopic through Bradford protein assay.

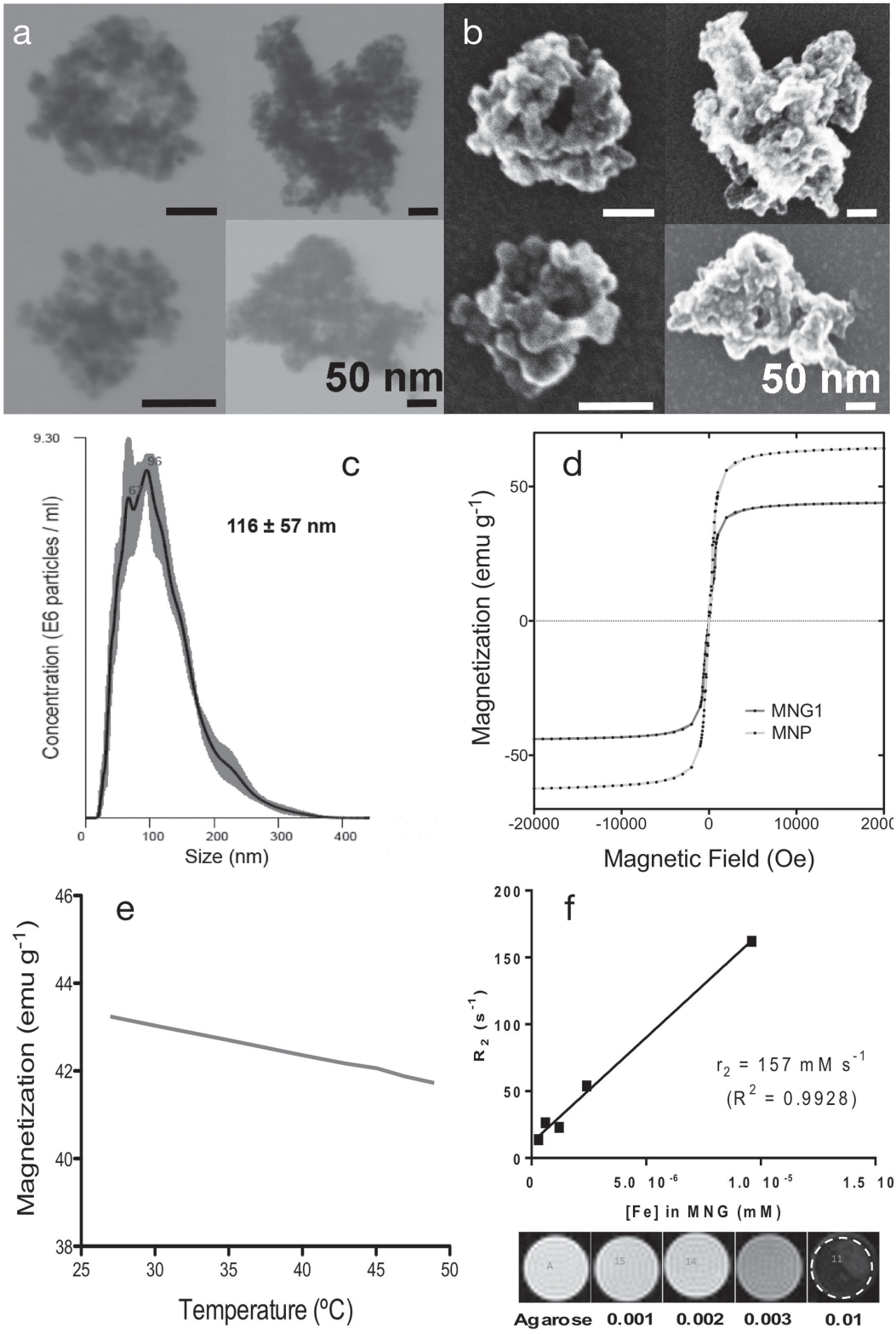

Figure 2. Size characteristics of a–c) **MNG4** and magnetic properties of c,d) **MNG1**. (a,b) TEM and SEM images of **MNG4**. (c) Hydrodynamic diameter distribution measured by NTA. (d) Magnetization curves of bare MNP and **MNG1** at 25 °C. e) Magnetization of MNG1 at 20 000 Oe with increasing temperature. f) T_2-weighted MRI images and MRI transverse relaxation times of **MNG1** at different concentrations.

Figure 2f, MNG1 transverse relaxations times ($R_2 = 1/T_2$) of different MNG concentrations were recorded. For the r_2 relaxivity, a value of $(157 \pm 10) \times 10^{-3}$ M^{-1} s^{-1} was obtained which lay in the range of such commercial available MRI contrasting agents as Feridex (120×10^{-3} M^{-1} s^{-1}) and Resovist (189×10^{-3} M^{-1} s^{-1}).[22] The transferrin content per MNG was determined via Bradford protein assay and was found to be 120, 7.6, and 9.3 nmol mg^{-1} for **MNG2**, **MNG3**, and **MNG4**, respectively (Table 1). The high Tf amount for **MNG2** could be traced back to a high **Tf-PEG$_4$–N$_3$** conjugation efficiency of 90% and a low overall reaction yield of only 33% in weight. **MNG3** and **MNG4** obtained moderate Tf amounts per mg MNG as the reaction yields were higher with values of 92 and 52 wt% (Table 1).

2.5. CTC Capturing Efficiencies of MNGs@Tf

For the evaluation of capturing efficiencies, **MNG@Tf** were mixed with human colon cancer HCT116-GFP (green fluorescence protein labeled) cells from an artificial CTCs suspension and isolated after 5 min through magnetic separation. The CTCs suspension consisted of spiked human peripheral blood mononuclear cells (hPBMC) cells (50×10^6 in 1 mL) with TfR^+ GFP-labelled HCT116 cells in various hPBMC:HCT116 ratios (e.g., 5×10^1:1, 2×10^2:1, 1×10^3:1, 2×10^3:1, 1×10^4:1 and 1×10^5:1) as reported earlier.[25] HCT116 cells were chosen for this study because they facilitated the identification and image-based counting of the target cells without further labelling with an imaging probe or by including cytokeratin (CK 18) antibody from a background of other blood cells. After paramagnetic isolation, both the captured and the remaining cell suspensions were imaged to estimate the number of captured and uncaptured HCT116-GFP cells in each sample. Figure S8 of the Supporting Information shows the fluorescence microscopy images of captured cells by **MNG@Tf** with different filters (Figure S8c, Supporting Information). Green fluorescence was only obtained for GFP-labeled cells (Figure S8 a, Supporting Information) while red fluorescence is observed for the **MNG@Tf** cluster as visualized in Figure S8b of the Supporting Information with rhodamine filter. The capturing efficiency was estimated with respect to the counted number of captured and uncaptured cells according to reported methodology.[34]

As shown in Figure 3, the distance between the nanogel and the attached Tf ligand had an influence on the obtained cell capture efficiency. Increasing the PEG chain length from four to eight ethylene glycol units caused an increment in capturing efficiency of 23% to 33%. Interestingly, a huge drop in the capturing ability to 7% was observed for the longest PEG linker length with 12 ethylene glycol units that was even lower than the control **MNG1** with no targeting ligand attached (Figure 3, Table 1). However, it could be concluded that an optimal PEG chain length was

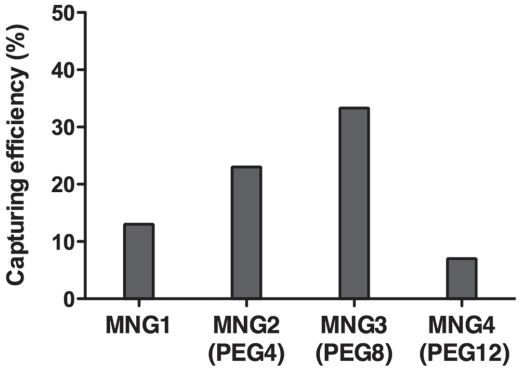

Figure 3. **MNG@Tf** cell capturing abilities as a function of the different lengths between the Tf ligand and the MNG.

required for enhancing cellular interactions of MNGs with epithelial cell adhesion molecules. The juxtaposition of Tf on this MNG platform was highly specific in its geometry and concentration. In addition, to the best of our knowledge, the current literature does not describe studies in this direction. The interplay between the optimal ligand distance and number of linkers per Tf will be explored in the future to reveal possible multivalent interactions and to improve capturing efficiencies.

3. Conclusions

We have demonstrated, in this study, a powerful methodology for the production of MNGs on the basis of an ultrasound assisted and strain-promoted copper-free crosslinking reaction. BCN modified magnetic nanoparticles and azide functionalized linear polyglycerol served as nanogel building blocks. Since our presented synthetic approach is based on a building block concept, it allows easy modification and substitution of targeting ligands as well as of polymer network chains and enables easy tuning of the size, flexibility, swelling capacity, and surface chemistry with ease. The obtained spherical MNGs were decorated with the model targeting ligand Tf and investigated for their magnetic cell catching ability on Tf receptor overexpressing cancer cells. Cell capture efficiency was found to be dependent on the distance between targeting ligand and MNG. Moreover, the MNGs magnetic relaxivity value was similar to commercial available contrasting agents for MRI. Hence, these results led to the conclusion that MNGs use is not limited for CTC capturing but can be extended for the use as a potential contrasting agent in MRI.

Supporting Information

Supporting Information is available from the Wiley Online Library or from the author.

Acknowledgements: M.A-.B. and C.B. contributed equally to this work. The authors thank the financial support of CONICET, SECyT-UNC, and FONCYT. M.C. thanks the collaborative research center SFB1112 (Project 04) and the NanoMatFutur award (13N12561) for financial support. M.C. and M.C.S. thank the cooperative research project sponsored by BMBF-Mincyt (2013) and Conicet-DFG (2014). J.B. acknowledges Dahlem Research Center for a Dahlem International Network PostDocs fellowship. The project was supported by the Freie Universität Berlin within the Excellence Initiative of the German Research Foundation. The authors acknowledge the focus area Nanoscale of the FU Berlin (http://www.nanoscale.fu-berlin.de). C.B. and A.C. thank CONICET and DAAD for the fellowship granted for her Ph.D. studies. Furthermore, the authors thank Pamela Winchester for language polishing of the manuscript.

Received: September 29, 2015; Revised: November 19, 2015; Published online: December 22, 2015; DOI: 10.1002/marc.201500590

Keywords: cell sorting; circulating tumor cells; thermoresponsive nanogels; transferrin

[1] K. Pantel, C. Alix-Panabières, *Trends Mol. Med.* **2010**, *16*, 398.
[2] J. Kaiser, *Science* **2010**, *327*, 1072.
[3] I. Lokody, *Nat. Rev. Cancer* **2014**, *14*, 152.
[4] M. G. Krebs, R. L. Metcalf, L. Carter, G. Brady, F. H. Blackhall, C. Dive, *Nat. Rev. Clin. Oncol.* **2014**, *11*, 129.
[5] S. Hou, H. Zhao, L. Zhao, Q. Shen, K. S. Wei, D. Y. Suh, A. Nakao, M. A. Garcia, M. Song, T. Lee, B. Xiong, S.-C. Luo, H.-R. Tseng, H.-H. Yu, *Adv. Mater.* **2013**, *25*, 1547.
[6] S. Nagrath, L. V. Sequist, S. Maheswaran, D. W. Bell, D. Irimia, L. Ulkus, M. R. Smith, E. L. Kwak, S. Digumarthy, A. Muzikansky, P. Ryan, U. J. Balis, R. G. Tompkins, D. A. Haber, M. Toner, *Nature* **2007**, *450*, 1235.
[7] M. Abonnenc, M. Borgatti, E. Fabbri, R. Gavioli, C. Fortini, F. Destro, L. Altomare, N. Manaresi, G. Medoro, A. Romani, M. Tartagni, E. Lo Monaco, P. Giacomini, R. Guerrieri, R. Gambari, *J. Immunol.* **2013**, *191*, 3545.
[8] S. Wang, K. Liu, J. Liu, Z. T.-F. Yu, X. Xu, L. Zhao, T. Lee, E. K. Lee, J. Reiss, Y.-K. Lee, L. W. K. Chung, J. Huang, M. Rettig, D. Seligson, K. N. Duraiswamy, C. K.-F. Shen, H.-R. Tseng, *Angew. Chem. Int. Ed.* **2011**, *50*, 3084.
[9] U. Dharmasiri, S. K. Njoroge, M. A. Witek, M. G. Adebiyi, J. W. Kamande, M. L. Hupert, F. Barany, S. A. Soper, *Anal. Chem.* **2011**, *83*, 2301.
[10] N. Saucedo-Zeni, S. Mewes, R. Niestroj, L. Gasiorowski, D. Murawa, P. Nowaczyk, T. Tomasi, E. Weber, G. Dworacki, N. G. Morgenthaler, H. Jansen, C. Propping, K. Sterzynska, W. Dyskiewicz, M. Zabel, M. Kiechle, U. Reuning, M. Schmitt, K. Luecke, *Int. J. Oncol.* **2012**, *41*, 1241.
[11] W. J. Allard, J. Matera, M. C. Miller, M. Repollet, M. C. Connelly, C. Rao, A. G. J. Tibbe, J. W. Uhr, L. W. M. M. Terstappen, *Clin. Cancer Res.* **2004**, *10*, 6897.
[12] A. H. Talasaz, A. A. Powell, D. E. Huber, J. G. Berbee, K.-H. Roh, W. Yu, W. Xiao, M. M. Davis, R. F. Pease, M. N. Mindrinos, S. S. Jeffrey, R. W. Davis, *Proc. Natl. Acad. Sci. USA* **2009**, *106*, 3970.
[13] C. Chen, M. Zimmermann, I. Tinhofer, A. M. Kaufmann, A. E. Albers, *Cancer Lett.* **2013**, *338*, 47.
[14] O. Veiseh, J. W. Gunn, M. Zhang, *Adv. Drug Delivery Rev.* **2010**, *62*, 284.
[15] A. E. Nel, L. Mädler, D. Velegol, T. Xia, E. M. V. Hoek, P. Somasundaran, F. Klaessig, V. Castranova, M. Thompson, *Nat. Mater.* **2009**, *8*, 543.
[16] L. Shang, K. Nienhaus, G. U. Nienhaus, *J. Nanobiotechnol.* **2014**, *12*, 5.
[17] I. Papp, C. Sieben, A. L. Sisson, J. Kostka, C. Böttcher, K. Ludwig, A. Herrmann, R. Haag, *ChemBioChem* **2011**, *12*, 887.
[18] S. E. A. Gratton, P. A. Ropp, P. D. Pohlhaus, J. C. Luft, V. J. Madden, M. E. Napier, J. M. DeSimone, *Proc. Natl. Acad. Sci. USA* **2008**, *105*, 11613.
[19] S. Mitragotri, J. Lahann, *Nat. Mater.* **2009**, *8*, 15.
[20] J. K. Oh, R. Drumright, D. J. Siegwart, K. Matyjaszewski, *Prog. Polym. Sci.* **2008**, *33*, 448.
[21] A. V. Kabanov, S. V. Vinogradov, *Angew. Chem. Int. Ed.* **2009**, *48*, 5418.
[22] M. Molina, M. Asadian-Birjand, J. Balach, J. Bergueiro, E. Miceli, M. Calderón, *Chem. Soc. Rev.* **2015**, *44*, 6161.
[23] T. Tsuji, H. Yoshitomi, J. Usukura, *Microscopy* **2013**, *62*, 341.
[24] E. Wagner, D. Curiel, M. Cotten, *Adv. Drug Delivery Rev.* **1994**, *14*, 113.
[25] S. S. Banerjee, A. Jalota-Badhwar, S. D. Satavalekar, S. G. Bhansali, N. D. Aher, R. R. Mascarenhas, D. Paul, S. Sharma, J. J. Khandare, *Adv. Healthcare Mater.* **2013**, *2*, 800.
[26] A. Burmistrova, M. Richter, C. Uzum, R. von Klitzing, *Colloid. Polym. Sci.* **2011**, *289*, 613.
[27] J. Wiedemair, M. J. Serpe, J. Kim, J.-F. Masson, L. A. Lyon, B. Mizaikoff, C. Kranz, *Langmuir* **2007**, *23*, 130.
[28] M. Weinhart, T. Becherer, N. Schnurbusch, K. Schwibbert, H. J. Kunte, R. Haag, *Adv. Eng. Mater.* **2011**, *13*, B501.
[29] R. K. Kainthan, J. Janzen, E. Levin, D. V. Devine, D. E. Brooks, *Biomacromolecules* **2006**, *7*, 703.
[30] A. Thomas, S. S. Müller, H. Frey, *Biomacromolecules* **2014**, *15*, 1935.
[31] M. Giulbudagian, M. Asadian-Birjand, D. Steinhilber, K. Achazi, M. Molina, M. Calderón, *Polym. Chem.* **2014**, *5*, 6909.
[32] J. Liu, C. Detrembleur, A. Debuigne, M.-C. De Pauw-Gillet, S. Mornet, L. Vander Elst, S. Laurent, E. Duguet, C. Jérôme, *J. Mater. Chem. B* **2014**, *2*, 1009.
[33] M. Bloemen, W. Brullot, T. T. Luong, N. Geukens, A. Gils, T. Verbiest, *J. Nanopart. Res.* **2012**, *14*, 1100.
[34] X. Zheng, L. S.-L. Cheung, J. A. Schroeder, L. Jiang, Y. Zohar, *Lab Chip* **2011**, *11*, 3269.